Atmos. Chem. Phys. Discuss., 13, 31713–31759, 2013
www.atmos-chem-phys-discuss.net/13/31713/2013/
doi:10.5194/acpd-13-31713-2013

Atmospheric Chemistry and Physics Discussions

Missing peroxy radical sources within a rural forest canopy

G. M. Wolfe[1,a,b], C. Cantrell[2,c], S. Kim[2,d], R. L. Mauldin III[2,3,c], T. Karl[2,e], P. Harley[2], A. Turnipseed[2], W. Zheng[2], F. Flocke[2], E. C. Apel[2], R. S. Hornbrook[2], S. R. Hall[2], K. Ullmann[2], S. B. Henry[1], J. P. DiGangi[1,f], E. S. Boyle[1], L. Kaser[4,g], R. Schnitzhofer[4], A. Hansel[4], M. Graus[5], Y. Nakashima[6,h], Y. Kajii[7], A. Guenther[2,i], and F. N. Keutsch[1]

[1]Department of Chemistry, University of Wisconsin, Madison, WI, USA
[2]Atmospheric Chemistry Division, National Center for Atmospheric Research, Boulder, CO, USA
[3]Department of Physics, University of Helsinki, Helsinki, Finland
[4]Institute of Ion Physics and Applied Physics, University of Innsbruck, Innsbruck, Austria
[5]Chemical Sciences Division, NOAA Earth System Research Laboratory, Boulder, CO, USA
[6]Division of Applied Chemistry, Faculty of Urban Environmental Sciences, Tokyo Metropolitan University, Tokyo, Japan
[7]Graduate School of Global Environmental Studies, Kyoto University, Kyoto, Japan
[a]now at: Joint Center for Earth Systems Technology, University of Maryland Baltimore County, Baltimore, MD, USA

[b]now at: Atmospheric Chemistry and Dynamics Laboratory, NASA Goddard Space Flight Center, Greenbelt, MD, USA
[c]now at: Department of Atmospheric and Oceanic Sciences, University of Colorado, Boulder, CO, USA
[d]now at: Department of Earth System Science, University of California, Irvine, CA, USA
[e]now at: Institute for Meteorology and Geophysics, University of Innsbruck, Innsbruck, Austria
[f]now at: Department of Civil & Environmental Engineering, Princeton University, Princeton, NJ, USA
[g]now at: Atmospheric Chemistry Division, National Center for Atmospheric Research, Boulder, CO, USA
[h]now at: Department of Environmental and Natural Resource Science, Faculty of Agriculture, Tokyo University of Agriculture and Technology, Tokyo, Japan
[i]now at: Atmospheric Sciences and Global Change Division, Pacific Northwest National Laboratory, Richland, WA, USA

Received: 29 October 2013 – Accepted: 25 November 2013 – Published: 4 December 2013

Correspondence to: G. M. Wolfe (zlonewolfe@gmail.com)

Published by Copernicus Publications on behalf of the European Geosciences Union.

Abstract

Organic peroxy (RO_2) and hydroperoxy (HO_2) radicals are key intermediates in the photochemical processes that generate ozone, secondary organic aerosol and reactive nitrogen reservoirs throughout the troposphere. In regions with ample biogenic hydrocarbons, the richness and complexity of peroxy radical chemistry presents a significant challenge to current-generation models, especially given the scarcity of measurements in such environments. We present peroxy radical observations acquired within a Ponderosa pine forest during the summer 2010 Bio-hydro-atmosphere interactions of Energy, Aerosols, Carbon, H_2O, Organics and Nitrogen – Rocky Mountain Organic Carbon Study (BEACHON-ROCS). Total peroxy radical mixing ratios reach as high as 180 pptv and are among the highest yet recorded. Using the comprehensive measurement suite to constrain a near-explicit 0-D box model, we investigate the sources, sinks and distribution of peroxy radicals below the forest canopy. The base chemical mechanism underestimates total peroxy radicals by as much as a factor of 3. Since primary reaction partners for peroxy radicals are either measured (NO) or under-predicted (HO_2 and RO_2, i.e. self-reaction), missing sources are the most likely explanation for this result. A close comparison of model output with observations reveals at least two distinct source signatures. The first missing source, characterized by a sharp midday maximum and a strong dependence on solar radiation, is consistent with photolytic production of HO_2. The diel profile of the second missing source peaks in the afternoon and suggests a process that generates RO_2 independently of sun-driven photochemistry, such as ozonolysis of reactive hydrocarbons. The maximum magnitudes of these missing sources ($\sim$ 120 and 50 pptv min^{-1}, respectively) are consistent with previous observations alluding to unexpectedly intense oxidation within forests. We conclude that a similar mechanism may underlie many such observations.

1 Introduction

Peroxy radicals are central components of the tropospheric radical pool. Organic peroxy radicals (RO_2) are metastable intermediates in the oxidation of volatile organic compounds (VOC), while hydroperoxyl radicals (HO_2) are generated via photolysis of carbonyl-containing VOC (e.g. formaldehyde), alkene ozonolysis and radical cycling reactions. RO_2 and HO_2 typically exhibit lifetimes of 1 to 1000 s with respect to reaction with nitric oxide (NO) and other peroxy radicals; larger RO_2 may also undergo isomerization and/or unimolecular decomposition. Together with the hydroxyl (OH) and alkoxy (RO) radicals, these species comprise the RO_x radical family. Rapid cycling among RO_x and the nitrogen oxide radicals (NO_x = NO + NO_2) lies at the core of photochemical mechanisms that regulate atmospheric composition and its associated impacts on air quality and climate.

$$\mathrm{VOC + OH \rightarrow RO_2} \quad \text{(R1)}$$

$$\mathrm{VOC} + h\nu \rightarrow \mathrm{HO_2 + products} \quad \text{(R2)}$$

$$\mathrm{VOC + O_3 \rightarrow HO_2 + products} \quad \text{(R3)}$$

$$\mathrm{RO_2 + NO \rightarrow RO + NO_2} \quad \text{(R4)}$$

$$\mathrm{HO_2 + NO \rightarrow OH + NO_2} \quad \text{(R5)}$$

$$\mathrm{RO + O_2 \rightarrow HO_2 + oVOC} \quad \text{(R6)}$$

$$\mathrm{HO_2 + HO_2 \rightarrow H_2O_2 + O_2} \quad \text{(R7)}$$

$$\mathrm{RO_2 + HO_2 \rightarrow ROOH + O_2} \quad \text{(R8)}$$

$$\mathrm{RO_2 + R'O_2 \rightarrow products} \quad \text{(R9)}$$

A number of key processes hinge upon the fate of peroxy radicals. For example, the conversion of NO to NO_2 via Reactions (R4) and (R5) is a critical step in tropospheric ozone formation (Thornton et al., 2002). Reactions of RO_2 with NO and NO_2 may also form alkyl nitrates and peroxy nitrates, respectively, facilitating the redistribution of pollutant precursors over regional and global scales (Moxim et al., 1996; Paulot

et al., 2012; Browne and Cohen, 2012). Conversely, cross-reactions of peroxy radicals (Reactions R7–R9) are responsible for termination of radical cycling in high-VOC, low-NO_x regimes. These reactions also form hydrogen peroxide (H_2O_2) and organic hydroperoxides (ROOH), which can induce oxidative stress in vegetation (Hewitt et al., 1990). Transformations of RO_2 also generate oxidized VOC that may contribute to formation and growth of secondary organic aerosol (SOA), a major fraction of the global aerosol burden (Hallquist et al., 2009). SOA precursor production depends strongly on the degree of functionalization vs. fragmentation (Chacon-Madrid and Donahue, 2011), which in turn varies with the specific molecular structure of each RO_2 radical. Peroxy radicals themselves can act as a major source of oxidants via Reaction (R5). Because this reaction shifts RO_x into its more reactive form while generating NO_2 (a precursor for ozone and thus OH), it effectively amplifies atmospheric oxidizing capacity. In many environments, this reaction is the main daytime source of OH (Stone et al., 2012).

The structure and abundance of VOC precursors shapes the detailed chemistry of peroxy radicals. In the remote troposphere, methane and CO are the primary reactants. Here, methyl peroxy radical (CH_3O_2) is the major RO_2 species and HO_2 concentrations typically exceed RO_2 (Cantrell et al., 2003). Near VOC sources, on the other hand, the RO_2 distribution can be considerably more complex and the prevailing chemistry is less well understood. This is particularly true in regions dominated by biogenic alkenes such as isoprene, 2-methyl-3-butene-2-ol (MBO) and monoterpenes. Numerous field studies have identified gaps in our understanding of photochemistry in these environments (Carslaw et al., 2001; DiGangi et al., 2011; Faloona et al., 2001; Griffith et al., 2012; Hofzumahaus et al., 2009; Lelieveld et al., 2008; Kim et al., 2013; Ren et al., 2008; Tan et al., 2001; Thornton et al., 2002; Whalley et al., 2011), while theoretical and laboratory work continues to reveal new reaction pathways that can significantly impact oxidant levels and reaction product distributions (Dillon and Crowley, 2008; Crounse et al., 2011, 2012; da Silva et al., 2010; Liu et al., 2012; Peeters and Müller, 2010; Peeters et al., 2009; Wolfe et al., 2012). Much of this work has focused on isoprene, which comprises one third of the global biogenic VOC emission budget (Guenther et al.,

2012). In most instances, uncertainties in these reaction mechanisms center on the fate of first-generation RO_2 and on processes that control the balance of OH, HO_2 and RO_2.

Observations of total peroxy radicals in forested environments are relatively sparse. During the ROSE campaign in rural Alabama, Cantrell et al. (1992, 1993) reported typical sunny mid-day $RO_2 + HO_2$ mixing ratios of 100 to 150 pptv in an isoprene-rich environment under minimal anthropogenic influence (NO ~ 100 pptv at noon). Maximum values of up to 300 pptv were observed on several days, and a steady-state model predicted an RO_2/HO_2 ratio of ~ 1 for one prototypical day. Qi et al. (2005) also observed fairly high $RO_2 + HO_2$ mixing ratios (109 to 134 pptv at midday) above a Japanese mixed deciduous forest with typical NO mixing ratios less than 200 pptv, and it was noted that peroxy radical concentrations consistently peaked ~ 3 h after solar noon. At the PROPHET site in Northern Michigan, Mihele and Hastie (2003) measured midday $RO_2 + HO_2$ ranging from 20 to 60 pptv. As in Qi et al. (2005), peroxy radicals at PROPHET were found to peak several hours after solar noon, indicating an important role for processes other than primary radical production. More recently, Griffith et al. (2012) reported midday mixing ratios of 20 to 50 pptv for the sum of HO_2 and first-generation isoprene peroxy radicals at PROPHET during summer of 2008 and 2009, consistent with earlier observations. Observations of HO_2 are more ubiquitous and are reviewed elsewhere (Stone et al., 2012), though some of these measurements may contain positive artifacts due to alkene-derived RO_2 (Fuchs et al., 2011). Investigations of RO_x cycling are often constrained with measurements of OH and HO_2 but rarely include a constraint on RO_2. Since RO_2 can comprise half or more of the total peroxy radical budget, such observations are crucial for identifying and eliminating gaps in chemical mechanisms.

We present an analysis of peroxy radical measurements obtained within a Ponderosa pine forest during the 2010 Bio–hydro–atmosphere interactions of Energy, Aerosols, Carbon, H_2O, Organics and Nitrogen – Rocky Mountain Organic Carbon Study (BEACHON-ROCS). Using the comprehensive suite of observations to constrain a near-explicit 0-D chemical box model, we examine the diel cycle of sources, sinks and

partitioning of peroxy radicals in this biogenic environment. Model underestimation of daytime peroxy radical concentrations leads us to consider potential missing radical sources. We quantify these missing processes and place them within the context of canonical chemistry. Analyzing the temporal profiles of missing peroxy radical mixing ratios and production rates, we identify potential novel mechanisms of radical generation that are consistent with previous anomalous observations at this and other forests.

2 Methods

2.1 Field campaign

BEACHON-ROCS took place from 1–31 August 2010 at the Manitou Forest Observatory (39°06′00″ N, 105°05′30″ W, 2286 m above sea level). The research site is situated within a Ponderosa pine forest with an average canopy height of 18.5 m and negligible undergrowth. A leaf area index (LAI) of 3 for the tree canopy and a tree cover fraction of 0.38 gives a landscape average LAI of 1.14. The closest major urban areas are Colorado Springs (33 km SE) and Denver (70 km N). The site is occasionally impacted by anthropogenic air masses, but prevailing winds bring relatively clean air from the south and southwest. Major biogenic VOC emissions at this site include 2-methyl-3-butene-2-ol (MBO), monoterpenes (MT) and methanol (Kaser et al., 2013a, b). Isoprene mixing ratios are typically less than 300 pptv, as this compound is only emitted from Ponderosa pine at very low rates (Kaser et al., 2013a). Further details on the site and observations can be found elsewhere (DiGangi et al., 2011, 2012; Karl et al., 2012; Kim et al., 2013; Kaser et al., 2013a, b).

2.2 Peroxy radical measurements

Two classes of peroxy radicals were measured via Peroxy Radical Chemical Ionization Mass Spectrometry (PeRCIMS), described in detail previously (Edwards et al., 2003; Hornbrook et al., 2011). The instrument was housed in a trailer on the forest floor with

the inlet protruding 0.5 m from the trailer wall at a height of 1.6 m and oriented to the southeast. The principle of detection involves three steps. First, ambient air is diluted with either N_2 or O_2, followed by addition of varying concentrations of NO and SO_2. Reaction of HO_2 with NO generates OH via Reaction (R5), while reaction of RO_2 with NO generates an RO radical that can react either with O_2 to form HO_2 via Reaction (R6) or with NO to make RONO.

$$RO + NO \rightarrow RONO \quad \text{(R10)}$$

Modulation of the NO/O_2 ratio controls the relative rates of Reactions (R6) and (R10) allowing the PeRCIMS to operate in either an HO_2 (high NO/O_2) or an $RO_2 + HO_2$ (low NO/O_2) measurement mode. The instrument switches between these two modes every 30 s. In the second and third steps, OH radicals react with SO_2 to generate sulfuric acid, which is then ionized via reaction with nitrate ions. Ions are detected via a custom-built quadrupole mass spectrometer.

$$OH + SO_2 + M + O_2 + 2H_2O \rightarrow\rightarrow H_2SO_4 + HO_2 + H_2O + M \quad \text{(R11)}$$

$$H_2SO_4 + NO_3^- \rightarrow HSO_4^- + HNO_3 \quad \text{(R12)}$$

Peroxy radical mixing ratios are reported as 1 min averages, with an uncertainty of ±35 % and a detection limit of 2 pptv for data from each measurement mode.

HO_2 measurements acquired via titration with NO can contain positive artifacts due to partial conversion of RO_2, especially when the RO_2 radicals are produced via OH addition to alkenes. The primary type of RO_2 interfering in the HO_2 measurement are likely β-hydroxyalkylperoxy radicals (βRO_2), formed via OH addition to alkenes (Fuchs et al., 2011; Hornbrook et al., 2011; Whalley et al., 2013). Upon reaction with NO in the PeRCIMS inlet, these radicals quickly decompose to make an HO_2 radical that is then detected with nearly the same efficiency as ambient HO_2. Laboratory experiments have shown that, relative to ambient HO_2, the PeRCIMS sensitivity to isoprene-derived RO_2 is ∼ 12 % higher, while that to aromatic RO_2 is ∼ 12 % lower (Hornbrook et al., 2011). Sensitivities to other β-hydroxyalkylperoxy radicals have not been tested, but

we assume their chemistry will be similar. For this reason, we define two quantities:

$$HO_2^* = HO_2 + \beta RO_2 \quad (1)$$

$$RO_2^* = HO_2 + RO_2 - HO_2^* \quad (2)$$

HO_2^* represents the "HO_2 mode" observations, which we assume to include HO_2 and βRO_2. RO_2^* denotes the difference between total peroxy radicals and HO_2^*, representing an operationally-defined subset of the RO_2 pool. The partitioning of total RO_2 between HO_2^* and RO_2^* is discussed further in Sects. 2.4 and 4.

2.3 Other measurements

Additional observations used in this analysis include OH, NO, NO_2, O_3, CO, PAN, PPN, formaldehyde, glyoxal, a suite of VOC (MBO, isoprene, α-pinene, β-pinene, limonene, camphene, non-speciated monoterpenes, acetone, methanol, benzene, toluene, methyl vinyl ketone, methacrolein, acetaldehyde, propanal, n-butanal, 1,3-butadiene), total OH reactivity, temperature, pressure, relative humidity and NO_2 photolysis frequencies. Table S1 in the Supplement (SI) summarizes the measurement techniques and their associated uncertainties. It should be noted that some measurements were taken at various heights, and the heterogeneity of the forest canopy can lead to strong vertical concentration gradients for some reactive species (Wolfe et al., 2011a). Furthermore, the openness of the MFO canopy can also leady to horizontal gradients in chemistry and composition. Most observations utilized here were taken at a height of 1.6–4 m, within the trunk space of the canopy. These heights are also listed in Table S1. NO_2 photolysis frequencies were measured both above the canopy and at 2 m (on top of the instrument trailer, just above the OH inlet). We caution that horizontally-averaged in-canopy radiation is likely higher than represented by this measurement, as the canopy is relatively open and the $J(NO_2)$ sensor was co-located with the relatively shaded OH inlet. Other photolysis frequencies, notably $J(O_3)$, are estimated by scaling measured $J(NO_2)$ with clear-sky photolysis frequencies calculated

from the Master Chemical Mechanism (MCM) v3.2 parameterization (Jenkin et al., 1997; Saunders et al., 2003).

VOC observations were acquired by four separate instruments, each with particular measurement heights, time resolution and speciation. A detailed comparison of these measurements is presented elsewhere (Kaser et al., 2013b). Due to better temporal coverage, MBO, benzene, toluene and acetaldehyde observations are taken from the University of Innsbruck PTR-TOF-MS measurements at 25 m. Remaining VOC listed above are taken from the NCAR trace organic gas analyzer (TOGA) measurements (also at 25 m). Furthermore, mixing ratios of MBO and monoterpenes, which are emitted by Ponderosa pine, are corrected for in-canopy gradients as described in the supplement. Vertical gradients of these compounds can be significant (up to 80 % change in mixing ratios between 4 and 23 m), thus this correction is a necessary step towards accurately representing in-canopy reactivity.

2.4 Model calculations

Detailed model calculations utilized the University of Washington Chemical Model (UWCM). This model incorporates a subset of the Master Chemical Mechanism (MCM) v3.2 (Jenkin et al., 1997; Saunders et al., 2003) with several updates and additional chemistry as detailed elsewhere (Wolfe and Thornton, 2011). Model setup is similar to that described by Kim et al. (2013) but with a few modifications. All input data are averaged to a 30 min diel cycle. Constraints include all observations listed above and constant mixing ratios of 1770 ppbv for CH_4 and 550 ppbv for H_2. The MCM mechanism subset includes all reactions from oxidation of MBO, isoprene, α-pinene, β-pinene, limonene, benzene, toluene, butadiene, acetaldehyde, propanal, n-butanal and methane. The simple MT mechanism of Wolfe and Thornton (2011) is used for camphene and unspeciated monoterpenes. Isomerization of first-generation isoprene peroxy radicals (Peeters and Müller, 2010; Peeters et al., 2009) is also included using measured rate coefficients for isomerization (Crounse et al., 2011) and subsequent loss of hydroperoxyaldehydes (Wolfe et al., 2012); recall that isoprene is, however,

a relatively minor contributor to VOC chemistry at this site. To account for cloud and forest cover, the ratio of in-canopy observed and MCM-calculated $J(NO_2)$ is used to generate a scaling factor, which is then applied to all MCM-parameterized photolysis frequencies. Some of our analysis below suggests that certain peroxy radicals may be sensitive to direct sunlight (Sect. 5.1); however, the attenuated light profile better represents photolytic sources of OH at the measurement location, and we use observations of this radical to test proposed mechanisms. Emissions and deposition are not explicitly considered, but an additional first-order loss process with a lifetime of 24 h is given to all species to represent physical losses (deposition and advection/dilution) and prevent buildup of long-lived products. The model is initialized at midnight and integrated for three days with observational constraints updated every 30 min. Three days is sufficient to reach a diurnal steady state, and results are shown from the third day. Specific model scenarios are described in the appropriate sections. Uncertainties in model mixing ratios are estimated from observational uncertainties as described in the Supplement.

Comparing model results with HO_2^* requires some assumptions regarding the contribution of organic peroxy radicals to this measurement. To first order, we assume that the HO_2^* measurement includes HO_2 and all first and second-generation β-hydroxyalkylperoxy radicals produced from OH oxidation of MBO, isoprene, monoterpenes, MVK, MACR, butadiene, benzene and toluene; specific radicals used are listed in Table S2.

3 Observations

The majority of peroxy radical measurements were collected during the final two weeks of the campaign (16–30 August). Figure S1 of the online supplement shows the full time series for peroxy radical mixing ratios, OH concentrations and meteorology. Meteorological conditions were warm and moderately dry (average mid-day temperature and relative humidity of $24 \pm 2\,^{\circ}C$ and $27 \pm 9\,\%$), with scattered clouds and occasional rain

after noon. Total peroxy radicals exhibited a regular diel cycle with daytime maxima of 100 to 180 pptv and nighttime minima of 0 to 10 pptv, within the range of observations from several other forest sites (Cantrell et al., 1992, 1993; Qi et al., 2005). HO_2^* tends to track total peroxy radicals, though the ratio of HO_2^* to total peroxy radicals (not shown) can vary significantly (from 0.4 to ~ 1) throughout the day. Daytime OH mixing ratios ranged from 3×10^6 to 10×10^6 molec cm^{-3}, while nighttime values were typically below the instrument detection limit of 5×10^5 molec cm^{-3}. Due to the regularity of diel cycles at this site and intermittent temporal overlap for many observations, our analysis will focus mainly on average diel behavior. All times discussed below refer to local solar time.

The mean diel cycle of peroxy radicals (Fig. 1) displays several interesting features. After sunrise, HO_2^* and $HO_2 + RO_2$ rise synchronously with both OH and O_3 photolysis frequency, consistent with photochemical sources. From 11:30 to 14:30, there is a sharp rise in HO_2^* and $HO_2 + RO_2$ that exceeds the smoother diel cycle seen in OH concentrations. This maximum, along with the brief spike at $\sim$ 15:30, are consistent daily features and not an averaging artifact. In the afternoon, the decay of HO_2^* is similar to that of OH, while $HO_2 + RO_2$ exhibits a shoulder that persists until $\sim$ 16:30. Nighttime peroxy radicals are low but consistently above the PeRCIMS detection limit of 2 pptv, with mean mixing ratios from midnight to 05:00 of 4 ± 2 pptv and 6 ± 2 pptv for HO_2^* and $HO_2 + RO_2$, respectively.

Figure 2 presents diel cycles for other key observations. Data are averaged over the full campaign (1–31 August). Though the degree of coverage varies for different species, most observations demonstrate consistent patterns from day to day. The sharp early morning rise in NO_x may be due to entrainment from aloft during the breakup of the nocturnal boundary layer (Seok et al., 2013) or surface emission (Alaghmand et al., 2011). The onset of this feature is synchronous with a rapid rise in ozone, likely attributable to the former mechanism. Observed daytime NO mixing ratios of 100–150 pptv are typical for a rural continental site and are within the transition region between "high" and "low" NO_x regimes, wherein both NO and other peroxy radicals

are expected to contribute significantly to total peroxy radical loss. MBO and monoterpenes, the primary emissions of Ponderosa pine, dominate the reactive VOC budget. Methanol is also abundant at this site (Kaser et al., 2013b), but it is relatively inert. Oxidation products, including formaldehyde, glyoxal and PAN, build up throughout the day, peaking in the late afternoon and decaying at night due to deposition, thermal decomposition and other losses. OH reactivity, a measure of the total OH loss rate, maintains a fairly constant value of 6–7 s^{-1} during the day and rises to as much 14 s^{-1} at night.

4 Model results

Two initial model scenarios are considered. In the first simulation, all observations other than peroxy radicals are used to constrain the model ("base"), while in a second simulation OH is determined by the model ("ModOH"). Figure 3 compares model output with RO_x observations for both scenarios, and additional model results are shown in the SI (Fig. S4). In the base case, total peroxy radicals are under-predicted throughout the day, with errors of up to a factor of 3 at midday. Un-constraining OH decreases mid-day modeled peroxy radicals by more than 50 %. The diel cycle of modeled peroxy radicals closely tracks that of OH in both scenarios. The morning rise in modeled and measured peroxy radical mixing ratios differs by several hours, suggesting a role for processes other than OH-driven VOC oxidation in early morning production. Moreover, the model captures neither the strong mid-day maximum nor the afternoon shoulder. In the ModOH scenario, OH concentrations are under-predicted throughout the day. This missing OH is likely at least partly due to an under-prediction of HO_2, which reduces the rate of OH production via Reaction (R5).

The relationship between OH and peroxy radicals is somewhat complicated by photochemical gradients and the role of vertical transport. Above the canopy, increased sunlight likely leads to more OH and thus more peroxy radicals, as demonstrated by a separate set of model runs constrained by above-canopy $J(NO_2)$ data (Fig. S5). Some of these radicals will be transported into the canopy, sustaining photochemistry

amidst attenuated radiation. To our knowledge, there are no published data comparing within and above-canopy peroxy radical levels; however, detailed 1-D canopy modeling results predict relatively minor gradients in HO_2 and total RO_2 at other forests (Bryan et al., 2012; Makar et al., 1999; Wolfe and Thornton, 2011; Wolfe et al., 2011a). For example, Wolfe and Thornton (2011) calculate that peroxy radical mixing ratios change by less than 10 % within a Ponderosa pine forest similar to that of BEACHON-ROCS. This may reflect the fact that decreased in-canopy production is balanced by downward mixing. Thus, model underestimates of peroxy radicals may be partly due to a missing source from downward transport, but only inasmuch as production and destruction rates vary between above and below-canopy environments. Moreover, the tight coupling of OH and HO_2 suggests that this phenomenon can be mostly accounted for by constraining OH to measurements. In this case, modeled peroxy radical mixing ratios are essentially independent of radiation (Fig. S5); in other words, OH-initiated chemistry is the dominant peroxy radical source in the model.

Under-prediction of OH reactivity could also lead to disagreement between modeled and measured peroxy radicals. Missing OH reactivity is a common feature of many studies in regions dominated by biogenic VOC (Lou et al., 2010; Edwards et al., 2013). A detailed analysis of OH reactivity at BEACHON–ROCS shows that measured species can only account for 41 % of the total OH reactivity on average, with poorer agreement at night (Nakashima et al., 2013). In the current study, the model underestimates total measured OH reactivity by as much as 20 % during the day and by 40 to 50 % at night for both scenarios (Fig. S4). It is important to note that unmeasured VOC oxidation products comprise a substantial fraction (up to 45 %) of the modeled OH reactivity, and the abundance of these compounds is highly sensitive to the assumed dilution rate of 1 day^{-1} (Edwards et al., 2013). For example, increasing the "physical loss" lifetime (Sect. 2.4) from 24 to 48 h increases modeled OH reactivity by $\sim 1\,s^{-1}$. Nonetheless, modeled and measured OH reactivity agree to within 20 % during the day, suggesting that the base model adequately represents the overall rate of OH-driven RO_2 production. This implies that other processes must also influence the peroxy radical budget.

Overall, modeled HO_2^* agrees somewhat better with observations than does total peroxy radicals, especially with OH constrained (Fig. 3c). Based on the above assumptions, HO_2 comprises 60–70 % of the modeled HO_2^*, giving peak midday modeled HO_2 mixing ratios of 25 and 12 pptv for the base and ModOH cases, respectively (Fig. S4). Roughly 50–60 % of total modeled RO_2 is produced from alkene oxidation (Fig. 4) and thus predicted to be detected as HO_2^*. The remainder, which we refer to as RO_2^*, can be compared with observations by taking the difference between measured $HO_2 + RO_2$ and HO_2^* (Fig. 3d). RO_2^* is generally underestimated, especially in the afternoon where the "shoulder" from $HO_2 + RO_2$ appears as a distinct peak. This feature is an important clue regarding the nature of missing RO_2.

The distribution of RO_2 radicals in the model closely follows that of VOC precursors (Fig. 4). MBO-derived RO_2 are the most abundant component during the day, while nighttime chemistry is dominated by monoterpenes, particularly β-pinene and limonene. This trend occurs for two reasons. First, MBO emissions are dependent upon both light and temperature (Harley et al., 1998), while monoterpene emissions at this site scale primarily with temperature (Kaser et al., 2013a), leading to different diel cycles in their concentrations (Fig. 2b). Secondly, MBO reacts almost exclusively with OH, while monoterpenes are reactive towards OH, O_3 and the nitrate radical (NO_3). The latter oxidant typically only accumulates at night (Fry et al., 2013). Our model results indicate similar contributions from OH and NO_3 chemistry to monoterpene oxidation in the first half of the night, with OH-driven loss prevailing in the early morning as NO_3 decays alongside its precursor, ozone. "Secondary" RO_2 arising from oxidation of unmeasured VOC comprise as much as 49 % of modeled RO_2, consistent with our earlier discussion of OH reactivity. HO_2 comprises 35–50 % of the total peroxy radical budget (Fig. 4). The diel cycle of $HO_2/(HO_2 + RO_2)$ is essentially the same for both model scenarios, demonstrating that absolute OH concentrations influence peroxy radical abundances but not partitioning. The mid-day minimum in this ratio reflects the increased importance of Reaction (R8) as a sink of HO_2 (see also Fig. 6).

In theory, model results can be used to estimate the contribution of HO_2 to HO_2^* observations. Several potential approaches are discussed in the SI. All of these methods inherently assume that model output faithfully represents the true peroxy radical distribution; however, without additional constraints on the nature of "missing" peroxy radicals, it is difficult to judge the reliability of this assumption. Thus, we elect to focus our analysis on the measured quantities, HO_2^* and RO_2^*.

5 Analysis and discussion

Discrepancies between modeled and observed peroxy radical mixing ratios indicate that the model is missing or misrepresenting sources and/or sinks of these species. Two features that stand out are the large midday maximum and the afternoon "shoulder", neither of which are captured by the model. Figure 5 quantifies this measurement-model mismatch. The magnitude of the model-measurement discrepancy should be interpreted with caution, as the combined uncertainties from model and observations leads to uncertainties of as much as a factor of 2 in the difference. Most of this uncertainty is systematic in nature (e.g. accuracy of calibrations), thus we have more confidence in the diurnal pattern of these differences. Interestingly, most of the under-prediction in HO_2^* arises from the midday maximum and the sharp afternoon satellite peak (Fig. 1), while RO_2^* under-prediction persists throughout the day and includes most of the broad afternoon shoulder. These features allude to multiple mechanistic issues, and we examine each observation separately.

5.1 Missing HO_2^*: a photolytic HO_2 source?

Understanding the nature of the midday HO_2^* maximum requires that we first determine whether this peak is primarily due to changes in HO_2 or RO_2. Given that (1) RO_2^* does not display a similar feature, and (2) we expect most RO_2 to exhibit similar diel cycles (Fig. 4), additional HO_2 production is the simplest explanation. Production of specific

RO_2 that contribute to HO_2^*, such as from photolysis of some yet-unidentified VOC, is also possible but less likely. This hypothesis implies several testable consequences, as detailed below.

To gauge the magnitude of this putative HO_2 source, we first examine the rates of HO_2 production and loss calculated from the 0-D model (Fig. 6). Reaction of RO_2 with NO comprises ~ 60 % of the modeled HO_2 source, with smaller contributions from photolysis and OH-reaction of oxidized VOC (mainly formaldehyde, HCHO). NO chemistry also dominates the loss of HO_2, though model underestimates of peroxy radical concentrations likely lead to an underestimate in the loss rates from reaction with HO_2 and RO_2. We can quantify the "missing" production rate by assuming that HO_2 is in steady state and calculating the loss rate of the missing HO_2:

$$P_{\text{miss}} = L_{\text{miss}} = [\text{HO}_2]_{\text{miss}} / \tau_{\text{HO}_2,\text{mod}} \quad (3)$$

Here, $[HO_2]_{miss}$ is the concentration of missing HO_2^* (Fig. 5) and $\tau_{HO_2,mod}$ is the lifetime of HO_2 calculated from the base model scenario. At its peak, the missing production rate is nearly double the total production rate from all known sources (Fig. 6, black line). For perspective, the maximum missing production rate of 102 ppt min^{-1} is 8 times the HO_2 production rate from reaction of MBO-derived RO_2 with NO and 24 times the production rate from HCHO photolysis. Reducing the HO_2 lifetime to account for under-predicted reaction rates with HO_2 and RO_2 (estimated using total peroxy radical measurements and the modeled HO_2/RO_2 ratio) increases P_{miss} by less than 20 %.

Increased HO_2 will provide an additional source of OH. Thus, as a further test, we incorporate this extra HO_2 source directly into the ModOH model scenario and compare model-calculated OH with observations (Fig. 7). This modification significantly increases daytime OH concentrations. Modeled OH generally agrees with observations (to within combined uncertainties) in the morning and afternoon hours but is over-predicted in the early afternoon, concomitant with the sharp HO_2^* maximum. The overall model-measurement agreement improves (slope = 0.25 vs 1.19, Fig. 7b), but the correlation degrades somewhat (r^2 = 0.81 vs. 0.75). These results suggest that such an

HO_2 radical source cannot be invoked without additional changes to the mechanism. Over-prediction of OH at the peak of extra HO_2 production likely indicates that some fraction of the missing HO_2^* is actually RO_2, counter to the simple assumption made above. Again, we caution that the magnitude of this missing HO_2^* source is highly uncertain. Furthermore, these results support the conclusion of Kim et al. (2013) that HO_2 can be a major source of OH in the canopy environment.

A closer analysis of the observational dataset provides further characterization of the missing source. Figure 8 shows an example of the relationship between peroxy radicals and solar radiation on 22 August; similar correlations were observed on many days of the campaign. Cloud cover regularly reduces direct sunlight at this site, decreasing above-canopy $J(NO_2)$ by factors of 2 to 4. Cloud effects on $J(NO_2)$ measured near the ground are comparatively minor since most of the radiation here is a combination of scattered diffuse light and occasional sun flecks (i.e. direct sun). In-canopy $J(NO_2)$ is a factor of 3 to 6 lower than above-canopy clear sky values (Fig. S5); we again caution that this is not necessarily representative of the "average" in-canopy environment (Sect. 2.3). HO_2^* increases to ~ 80 pptv from 11:30 to 14:30, consistent with the midday maximum in the diel average; however, HO_2^* also decreases rapidly during periods of sustained radiation attenuation, down to levels similar to those observed before and after the maximum. RO_2^* exhibits some correlation with above-canopy radiation (e.g. the troughs at hours 12:40 and 15:00), but generally the correlation is weaker and variations in RO_2^* are more independent of radiation. These trends are also borne out in the broader statistics of the full dataset (Fig. S7). The difference in the radiation dependence of HO_2^* and RO_2^* suggests that fast changes in HO_2^* are not solely driven by the radiation dependence of OH.

The simplest explanation for the observed behavior is production of peroxy radicals from gas-phase oxidation and/or photolysis of VOC. Additional production from OH chemistry is unlikely, as the model is constrained by measured OH and reproduces observed OH reactivity to within 20 % during the day (Fig. S4). Only a handful of VOC are known to exclusively produce HO_2 during OH oxidation, notably formaldehyde (HCHO)

and glyoxal (HCOCHO), both of which are constrained by observations in our model. Gas-phase photolysis of an unidentified compound is another potential explanation, though the emission (or production) of such a molecule would need to match the unique profile of the HO_2^* midday maximum (Fig. 5). None of the other 213 meteorological and chemical observations resemble this profile, thus we have no additional clues as to the nature of this source. HO_2 production from reactions of "missing" RO_2^* with NO may also explain some of the missing HO_2^*, but not the mid-day maximum (see Sect. 5.2 and Fig. 11).

Numerous investigations have inferred the presence of significant unidentified reactive hydrocarbons in biogenic environments. Often this conclusion arises from discrepancies between measured and calculated OH reactivity (Di Carlo et al., 2004; Edwards et al., 2013; Lou et al., 2010; Sinha et al., 2010; Nölscher et al., 2012). It is still debated whether the missing reactivity is due to primary emissions or secondary oxidation products, though this likely varies from site to site. While under-represented OH reactivity could have a profound impact on peroxy radical chemistry elsewhere, we reiterate that this is not a viable explanation for missing peroxy radicals in the present study. Fast downward ozone fluxes (Goldstein et al., 2004; Kurpius and Goldstein, 2003) and high levels of oxidized VOC (Holzinger et al., 2005) have also been taken as evidence for unconventional in-canopy chemistry. Both of these findings originate from observations in a Ponderosa pine ecosystem similar to Manitou Experimental Forest, thus it is conceivable that similar chemistry is at play. Perhaps the most relevant line of evidence for the present study is the observation of unexpectedly large upward fluxes of HCHO during BEACHON-ROCS (DiGangi et al., 2011). Formaldehyde is a major product from the oxidation of nearly every VOC and is thus an excellent tracer for the overall efficiency of hydrocarbon degradation. DiGangi et al. (2011) demonstrated that a simple mass balance model incorporating known chemical and physical processes under-predicted the observed HCHO flux by a factor of 6. The investigators concluded that the missing HCHO source could be attributed to oxidation of unidentified biogenic VOC and/or

direct emissions of HCHO from vegetation. In either case, closure of the HCHO flux budget required that the missing process correlate with solar radiation.

It is possible that the missing sources of HCHO and HO_2^* are related. The maximum "missing" HCHO flux of $\sim 20\,\mathrm{pptv\,m\,s^{-1}}$ corresponds to an in-canopy HCHO production rate of $65\,\mathrm{pptv\,min^{-1}}$ (for a canopy height of 18.5 m), within the range of the missing HO_2^* source (Fig. 6). Candidate precursors for both HCHO and HO_2 are methylperoxy, hydroxymethyl and β-hydroxyalkoxy radicals, which decompose rapidly under normal atmospheric conditions:

$$CH_3O^\bullet + O_2 \rightarrow HCHO + HO_2 \quad \text{(R13)}$$

$$^\bullet CH_2OH + O_2 \rightarrow HCHO + HO_2 \quad \text{(R14)}$$

$$RR'C(O^\bullet)CH_2OH + O_2 \rightarrow HCHO + HO_2 + RC(O)R' \quad \text{(R15)}$$

The lifetimes of these radicals are so short that the above reactions are often assumed to be instantaneous. In conventional chemical mechanisms, these radicals are intermediates of peroxy radical decomposition (mainly via reaction with NO). While known photolytic sources for such molecules are thought to be minor, it is possible that photolysis of yet-unidentified VOC could simultaneously stimulate production of both HCHO and HO_2, which in turn would accelerate HO_x-driven photochemistry within and above the forest canopy.

5.2 Missing RO_2^*: evidence for unidentified VOC?

In contrast to HO_2^*, missing RO_2^* mixing ratios exhibit a relatively smooth diel cycle (Fig. 5). This signal comprises most of the total missing peroxy radicals in the morning and afternoon, with a maximum at ~ 16:00. The shape of the diel profile is notably similar to that of several oxidation products, including HCHO, glyoxal and PAN (Fig. 2c). Many modeled oxidation products, including first-generation peroxides and organic nitrates, also peak at this time (not shown). RO_2 sinks are dominated by reaction with NO (Fig. 9), and under-prediction of HO_2 in the base simulation likely results in under-

estimation of RO_2 loss via reaction with HO_2. Thus, missing RO_2^* reflects an issue with RO_2 sources.

We can estimate the magnitude of the missing RO_2^* source using an approach similar to that described for HO_2^* (Eq. 3). This method requires calculation of the missing RO_2^* lifetime; however, this value depends on the assumed structure of these peroxy radicals. Figure 9a illustrates this point for three representative peroxy radicals. The lifetime of CH_3O_2 and MBOAO2 (the primary RO_2 from MBO oxidation) ranges from 30 to 60 s throughout the day, except in the morning when NO concentrations spike (Fig. 2a). In contrast, the lifetime of the acetyl peroxy radical, CH_3CO_3, is typically < 20 s. These differences arise mainly from NO reaction rate constants, which are 7.7, 9.0 and 20×10^{-12} $cm^3\,molec^{-1}\,s^{-1}$ at 298 K for CH_3O_2, MBOAO2 and CH_3CO_3, respectively. Reaction with HO_2 can also be an important sink for MBOAO2 (Fig. 10a) and other large peroxy radicals. For comparison, we also show the concentration-weighted average RO_2^* lifetime for all model species in the RO_2^* group. Coincidentally, this lifetime is nearly identical to that of MBOAO2 even though this radical is not included in RO_2^*. Figure 9b compares the total production rate of modeled RO_2^* with missing RO_2^* production rates as calculated via Eq. (3). The magnitude of the missing production rate is similar to that of the "known" production rate except when RO_2^* is assumed to have a lifetime comparable to CH_3CO_3. In the latter instance, the source strength needed to explain missing RO_2^* often exceeds the largest values estimated for missing HO_2^* (Fig. 6). For the other three cases, missing RO_2^* production follows a diurnal pattern similar to its concentration profile (Fig. 5c) except in the morning, where the steady-state assumption may be invalid due to rapidly-changing NO concentrations. Recall that the absolute magnitude of this source is dependent on our estimate of missing RO_2^* and thus is highly uncertain.

The contrast between diurnal cycles of production rates for "known" and missing RO_2^* (Fig. 9b) demonstrates that the processes driving missing RO_2^* are not solely sun-driven (i.e. OH reaction with VOC). Figure 10 shows modeled tendencies for the same three representative RO_2 species (MBOAO2, CH_3O_2 and CH_3CO_3). Overall radical

production tends to track with solar radiation, but some processes exhibit minor diurnal asymmetry. In particular, production of CH_3O_2 and CH_3CO_3 radicals from reactions of other RO_2 with NO maximizes slightly after noon due to both an increase in NO (Fig. 2a) and the buildup of RO_2. Despite these features, OH is still the main driver for classical RO_2 production, and none of the 347 modeled RO_2 species exhibit a profile similar to that of the missing RO_2^*. While amplification of a purely OH or light-dependent process may be able to explain missing RO_2^* in the morning, such a source cannot explain the afternoon maximum. These results lead us to consider other non-OH RO_2 sources that may be under-represented in the model mechanism.

One potential candidate for missing RO_2^* is the acyl peroxy (AP) radical family. AP radicals are a special class of peroxy radical that can react with NO_2 to form a metastable acyl peroxy nitrate (APN):

$$RC(O)O_2 + NO_2 \rightleftarrows RC(O)O_2NO_2 \text{ (APN)} \quad \text{(R16)}$$

Temperature controls the lifetime of APNs; for the conditions of BEACHON-ROCS (4 to 29 °C), the lifetime of PAN ranges from 23 h to 24 min. APNs can act as a source or sink of AP radicals depending on equilibrium conditions and the strength of primary AP sources (LaFranchi et al., 2009). Our model predicts that PAN, the most abundant APN, is a net sink for acetyl peroxy radicals (Fig. 10c); however, the net rate of CH_3CO_3 loss via PAN formation is small compared to primary CH_3CO_3 production and reaction with NO, indicating near-steady state conditions (Cleary et al., 2007; LaFranchi et al., 2009). Moreover, the model predicts a number of additional APNs, with PAN (which is constrained by observations) comprising only 19–39 % of the total budget. The next most abundant APN is the MCM species C4PAN5, a byproduct of MBO oxidation, at 17–22 %. The shape of the missing RO_2^* profile may imply an under-estimation in the source of AP radicals from decomposition of such APNs. Assuming steady state conditions for APNs, the AP radical concentration from this source alone is given by

$$[AP] = \frac{k_{18r}[APN]}{k_{18f}[NO_2]} \quad (4)$$

where k_{18r} and k_{18f} are the reverse and forward rate constants for Reaction (R16). Based on this equation, errors in APN concentrations or reaction rates could lead to under-prediction of AP radicals. Errors in APN concentrations are likely not a viable explanation. Evidence from other investigations suggests that > 90 % of the total peroxy nitrate budget is comprised of only a handful of APNs, mostly PAN (Wooldridge et al., 2010); thus, it is likely that modeled APN concentrations are already over-estimated. Errors in rate constants are more probable, as MCM rate constants for APN formation and loss are assumed equal to that of PAN, except for decomposition of PPN and MPAN, which follow IUPAC recommendations (Jenkin et al., 1997; Saunders et al., 2003). Laboratory data from Kirchner et al. (1999) indicate that decomposition rates generally decrease with increasing size and decreasing electronegativity of the organic functional group. In contrast, IUPAC recommends decomposition rate constants for PPN and MPAN that are ∼ 10 % faster than that of PAN. Formation rate constants have not been measured for species other than PAN, though one study has suggested that PPN formation may be 11 % slower than that of PAN (Sommariva et al., 2011). To completely explain missing RO_2^*, we estimate that the equilibrium constant (k_{18f}/k_{18r}) for model APNs would need to decrease by more than a factor of 10, well beyond the likely uncertainty in this value. Moreover, model simulations show that most of the growth in the RO_2 pool from such a change is due not to AP radicals themselves but rather to the RO_2 products of the reaction of AP with NO. Thus, we conclude that AP radicals are not a major component of missing RO_2^*.

Other RO_2^* generation mechanisms to consider include reaction of VOC with ozone or nitrate radical (NO_3). In the base model simulation, ozone chemistry contributes 10–20 % to the daytime peroxy radical budget, while NO_3 chemistry is only significant at night. Ozonolysis of unidentified VOC has been invoked previously to explain anomalously high ozone fluxes (Goldstein et al., 2004; Hogg et al., 2007; Kurpius and Goldstein, 2003), oxidation product concentrations (Holzinger et al., 2005) and sulfuric acid levels (Mauldin et al., 2012) in other forests. Decomposition of Criegee intermediates can simultaneously generate OH and RO_2 radicals, with measured yields ranging from

0.06 to near-unity (Aschmann et al., 2002; Atkinson and Arey, 2003; Shu and Atkinson, 1994). In a detailed modeling study, Wolfe et al. (2011b) established an upper limit for RO_2 production from ozonolysis of "very reactive" VOC of 60 pptv min^{-1}, similar to both our missing RO_2^* source and the missing HCHO source inferred by DiGangi et al. (2011). The latter study also determined that any missing VOC should exhibit a light-dependent emission profile similar to that of MBO.

To test this hypothesis, we implement an additional set of reactions following the very reactive VOC mechanism described by Wolfe et al. (2011b). Specific reactions are listed in Table S3. Rate constants for initial oxidation of this hypothetical VOC are assumed equal to those of β-caryophyllene, while reactions of the peroxy radical products are assumed to be similar to those of the β-pinene-derived radical BPINAO2. As a modification to the original mechanism, we discriminate between RO_2 made by OH, O_3 and NO_3 chemistry, since we anticipate that OH-derived RO_2 would be detected as HO_2^* in the PeRCIMS inlet. The yield of OH and RO_2 from ozonolysis is set to the upper limit of 0.1 recommended by Wolfe et al. (2011b). Very reactive VOC mixing ratios, shown in Fig. S8, are fixed to a diurnal cycle that scales with the observed flux of the sum of MBO and isoprene (Kaser et al., 2013a). The scaling factor of 0.23 is chosen to optimize model-measurement agreement for total peroxy radicals in the base scenario. We caution that inferred VRVOC mixing ratios depend directly on the assumed reaction rate constants and product yields – the product of which determines the RO_2 production rate. In other words, this calculation effectively constrains the VRVOC reactivity, as discussed in Wolfe et al. (2011b). We implement this mechanism for both the base and ModOH scenarios; results are shown in Fig. 11. Model-measurement agreement for all radicals improves markedly on incorporating very reactive VOC chemistry (compare to Fig. 3), though the unique diurnal patterns of HO_2^* and RO_2^* are not captured. With OH constrained to observations, model agreement with HO_2^* improves due to (1) RO_2 from reaction of very reactive VOC with OH and (2) increased HO_2 from reaction of new RO_2 radicals with NO. With OH determined by the model, however, HO_2^* is over-predicted in the afternoon. This is mainly driven by excess OH co-produced with RO_2

during ozonolysis of very reactive VOC. On the other hand, the latter fraction of RO2 also improves agreement with RO_2^*. Thus, the ozonolysis of unidentified hydrocarbons alone cannot provide closure of the RO_x budget unless (1) OH is not produced with the same yield as RO_2, contrary to canonical mechanisms, or (2) additional processes are invoked that affect the diel OH profile. Nonetheless, these results strongly support an intimate chemical link between missing peroxy radicals and other yet-unexplained observations (i.e. HCHO and ozone fluxes) within the canopy airspace.

6 Conclusions

Using the comprehensive suite of observations from the 2010 BEACHON-ROCS field campaign, we have explored the detailed chemistry of peroxy radicals in a rural environment dominated by biogenic hydrocarbons. Total peroxy radical concentrations are among the highest yet reported, exceeding 100 pptv on every day of observations and reaching as high as 180 pptv. Box model calculations under-predict total peroxy radicals by as much as a factor of 3, indicative of missing sources. Though the PeRCIMS instrument does not provide a strict segregation between HO_2 and RO_2 radicals, the data alludes to several distinct sources. High levels of HO_2^* at mid-day, combined with a clear dependence on radiation and a lack of similar behavior in RO_2^*, suggest a missing photolytic source of HO_2. The magnitude of this missing source is highly uncertain, and its exact nature remains a mystery. RO_2^* is also under-predicted, but the diel profile of missing RO_2^* more closely resembles that of oxidation products and light-dependent VOC emissions. Implementing an additional chemical mechanism involving ozonolysis of putative "very reactive" VOC greatly improves model-measurement agreement with all radicals. With OH determined by the model, this same mechanism degrades agreement with measured OH and HO_2^* unless the OH yield is assumed to be lower than the RO_2 yield, contrary to classical chemistry. While these results do not provide closure of the radical budget, they do imply that similar mechanisms may underlie both missing

peroxy radicals and other indicators of faster-than-expected chemistry at this and other forests.

Failure to accurately represent peroxy radical chemistry in biogenic regimes will limit the reliability of model results and predictions. For example, the impact of peroxy radicals on ozone production is a complex balance between the NO turnover rate and the production of radical reservoirs, such as alkyl nitrates and peroxy acyl nitrates. Modeled production of such compounds depends directly on the calculated RO_2 distribution, and changing the assumed yield of NO_x reservoir species can alter ozone production on regional and larger scales (Farmer et al., 2011; Paulot et al., 2012). Inter-conversion of reactive nitrogen also affects estimates of nitrogen deposition, which represents a critical link between atmospheric composition and ecosystem health (Sparks et al., 2008). Peroxy radical chemistry is also intimately tied to atmospheric oxidizing capacity. In environments where HO_2 is a dominant precursor of OH, missing peroxy radical sources will lead to underestimation of the overall rate of oxidation. Understanding this chemistry is particularly critical in high-VOC, low-NO_x regimes where radical cycling is controlled by $RO_x + HO_2$ reactions and, potentially, unimolecular decomposition of larger RO_2 (Archibald et al., 2010; Stavrakou et al., 2010). For all these reasons, it is imperative that we identify and eliminate remaining gaps in our understanding of chemistry in such environments – especially if mechanistic shortcomings are as substantial as implied by this study.

Closure of the RO_x budget will require a comprehensive understanding of both primary radical sources and the processes that control radical cycling in the continental boundary layer. Of critical importance is continued measurement of organic peroxy radicals, as these are too often a key missing constraint in modeling studies. Further speciation of these compounds would also greatly aid identification of errors in current chemical mechanisms. While it may not yet be technically feasible to segregate all individual RO_2, progress could be made by determining the distribution of different RO_2 families (i.e. acyl peroxy, β-hydroxyalkylperoxy, etc.). Measurements of radical reservoirs and termination products, such as organic peroxides (ROOH) and alkyl nitrates

($RONO_2$), will also play a vital role in this regard. Observations of total ozone production (Cazorla and Brune, 2010) may also provide a useful check on observations of total peroxy radical concentrations while offering an integrated perspective on pertinent chemistry in biogenic environments.

Supplementary material related to this article is available online at http://www.atmos-chem-phys-discuss.net/13/31713/2013/acpd-13-31713-2013-supplement.pdf.

Acknowledgements. The National Center for Atmospheric Research is operated by the University Corporation for Atmospheric Research under sponsorship from the US National Science Foundation. Any opinions, findings and conclusions or recommendations expressed in this publication are those of the authors and do not necessarily reflect the views of the National Science Foundation. The authors also thank the National Science Foundation (ATM 0852406) and the Austrian Science Fund (FWF) under the project number L518-N20. Lisa Kaser is a recipient of a DOC-fFORTE-fellowship of the Austrian Academy of Sciences at the Institute of Ion Physics and Applied Physics. This work was also supported by the EC Seventh Framework Program (Marie Curie Reintegration Program, "ALP-AIR", grant no. 334084) to T. Karl. G. M. Wolfe acknowledges support from the NOAA Climate and Global Change Postdoctoral Fellowship Program. Finally, we thank the US Forest Service, specifically Richard Oakes, for logistical support.

References

Alaghmand, M., Shepson, P. B., Starn, T. K., Jobson, B. T., Wallace, H. W., Carroll, M. A., Bertman, S. B., Lamb, B., Edburg, S. L., Zhou, X., Apel, E., Riemer, D., Stevens, P., and Keutsch, F.: The Morning NO_x maximum in the forest atmosphere boundary layer, Atmos. Chem. Phys. Discuss., 11, 29251–29282, doi:10.5194/acpd-11-29251-2011, 2011.

Archibald, A. T., Cooke, M. C., Utembe, S. R., Shallcross, D. E., Derwent, R. G., and Jenkin, M. E.: Impacts of mechanistic changes on HO_x formation and recycling in the oxidation of isoprene, Atmos. Chem. Phys., 10, 8097–8118, doi:10.5194/acp-10-8097-2010, 2010.

Aschmann, S. M., Arey, J., and Atkinson, R.: OH radical formation from the gas-phase reactions of O_3 with a series of terpenes, Atmos. Environ., 36, 4347–4355, 2002.

Atkinson, R. and Arey, J.: Atmospheric degradation of volatile organic compounds, Chem. Rev., 103, 4605–4638, 2003.

Browne, E. C. and Cohen, R. C.: Effects of biogenic nitrate chemistry on the NO_x lifetime in remote continental regions, Atmos. Chem. Phys., 12, 11917–11932, doi:10.5194/acp-12-11917-2012, 2012.

Bryan, A. M., Bertman, S. B., Carroll, M. A., Dusanter, S., Edwards, G. D., Forkel, R., Griffith, S., Guenther, A. B., Hansen, R. F., Helmig, D., Jobson, B. T., Keutsch, F. N., Lefer, B. L., Pressley, S. N., Shepson, P. B., Stevens, P. S., and Steiner, A. L.: In-canopy gas-phase chemistry during CABINEX 2009: sensitivity of a 1-D canopy model to vertical mixing and isoprene chemistry, Atmos. Chem. Phys., 12, 8829–8849, doi:10.5194/acp-12-8829-2012, 2012.

Cantrell, C. A., Lind, J. A., Shetter, R. E., Calvert, J. G., Goldan, P. D., Kuster, W., Fehsenfeld, F. C., Montzka, S. A., Parrish, D. D., Williams, E. J., Buhr, M. P., Westberg, H. H., Allwine, G., and Martin, R.: Peroxy-radicals in the ROSE experiment – measurement and theory, J. Geophys. Res.-Atmos., 97, 20671–20686, 1992.

Cantrell, C. A., Shetter, R. E., Calvert, J. G., Parrish, D. D., Fehsenfeld, F. C., Goldan, P. D., Kuster, W., Williams, E. J., Westberg, H. H., Allwine, G., and Martin, R.: Peroxy radicals as measured in ROSE and estimated from photostationary state deviations, J. Geophys. Res., 98, 18355–18366, 1993.

Cantrell, C. A., Mauldin, L., Zondlo, M., Eisele, F., Kosciuch, E., Shetter, R., Lefer, B., Hall, S., Campos, T., Ridley, B., Walega, J., Fried, A., Wert, B., Flocke, F., Weinheimer, A., Hannigan, J., Coffey, M., Atlas, E., Stephens, S., Heikes, B., Snow, J., Blake, D., Blake, N., Katzenstein, A., Lopez, J., Browell, E. V., Dibb, J., Scheuer, E., Seid, G., and Talbot, R.: Steady state free radical budgets and ozone photochemistry during TOPSE, J. Geophys. Res.-Atmos., 108, 8361, doi:10.1029/2002JD002198, 2003.

Carslaw, N., Creasey, D. J., Harrison, D., Heard, D. E., Hunter, M. C., Jacobs, P. J., Jenkin, M. E., Lee, J. D., Lewis, A. C., Pilling, M. J., Saunders, S. M., and Seakins, P. W.: OH and HO2 radical chemistry in a forested region of north-western Greece, Atmos. Environ., 35, 4725–4737, 2001.

Cazorla, M. and Brune, W. H.: Measurement of Ozone Production Sensor, Atmos. Meas. Tech., 3, 545–555, doi:10.5194/amt-3-545-2010, 2010.
Chacon-Madrid, H. J. and Donahue, N. M.: Fragmentation vs. functionalization: chemical aging and organic aerosol formation, Atmos. Chem. Phys., 11, 10553–10563, doi:10.5194/acp-11-10553-2011, 2011.
Cleary, P. A., Wooldridge, P. J., Millet, D. B., McKay, M., Goldstein, A. H., and Cohen, R. C.: Observations of total peroxy nitrates and aldehydes: measurement interpretation and inference of OH radical concentrations, Atmos. Chem. Phys., 7, 1947–1960, doi:10.5194/acp-7-1947-2007, 2007.
Crounse, J. D., Paulot, F., Kjaergaard, H. G., and Wennberg, P. O.: Peroxy radical isomerization in the oxidation of isoprene, Phys. Chem. Chem. Phys., 13, 13607–13613, 2011.
Crounse, J. D., Knap, H. C., Ørnsø, K. B., Jørgensen, S., Paulot, F., Kjaergaard, H. G., and Wennberg, P. O.: On the atmospheric fate of methacrolein: 1. Peroxy radical isomerization following addition of OH and O_2, J. Phys. Chem. A, 116, 5756–5762, doi:10.1021/jp211560u, 2012.
da Silva, G., Graham, C., and Wang, Z. F.: Unimolecular beta-hydroxyperoxy radical decomposition with OH recycling in the photochemical oxidation of isoprene, Environ. Sci. Technol., 44, 250–256, 2010.
Di Carlo, P., Brune, W. H., Martinez, M., Harder, H., Lesher, R., Ren, X. R., Thornberry, T., Carroll, M. A., Young, V., Shepson, P. B., Riemer, D., Apel, E., and Campbell, C.: Missing OH reactivity in a forest: evidence for unknown reactive biogenic VOCs, Science, 304, 722–725, 2004.
DiGangi, J. P., Boyle, E. S., Karl, T., Harley, P., Turnipseed, A., Kim, S., Cantrell, C., Maudlin III, R. L., Zheng, W., Flocke, F., Hall, S. R., Ullmann, K., Nakashima, Y., Paul, J. B., Wolfe, G. M., Desai, A. R., Kajii, Y., Guenther, A., and Keutsch, F. N.: First direct measurements of formaldehyde flux via eddy covariance: implications for missing in-canopy formaldehyde sources, Atmos. Chem. Phys., 11, 10565–10578, doi:10.5194/acp-11-10565-2011, 2011.
DiGangi, J. P., Henry, S. B., Kammrath, A., Boyle, E. S., Kaser, L., Schnitzhofer, R., Graus, M., Turnipseed, A., Park, J-H., Weber, R. J., Hornbrook, R. S., Cantrell, C. A., Maudlin III, R. L., Kim, S., Nakashima, Y., Wolfe, G. M., Kajii, Y., Apel, E.C., Goldstein, A. H., Guenther, A., Karl, T., Hansel, A., and Keutsch, F. N.: Observations of glyoxal and formaldehyde as metrics

for the anthropogenic impact on rural photochemistry, Atmos. Chem. Phys., 12, 9529–9543, doi:10.5194/acp-12-9529-2012, 2012.
Dillon, T. J. and Crowley, J. N.: Direct detection of OH formation in the reactions of HO_2 with $CH_3C(O)O_2$ and other substituted peroxy radicals, Atmos. Chem. Phys., 8, 4877–4889, doi:10.5194/acp-8-4877-2008, 2008.
Edwards, G. D., Cantrell, C. A., Stephens, S., Hill, B., Goyea, O., Shetter, R. E., Mauldin, R. L., Kosciuch, E., Tanner, D. J., and Eisele, F. L.: Chemical ionization mass spectrometer instrument for the measurement of tropospheric HO_2 and RO_2, Anal. Chem., 75, 5317–5327, 2003.
Edwards, P. M., Evans, M. J., Furneaux, K. L., Hopkins, J., Ingham, T., Jones, C., Lee, J. D., Lewis, A. C., Moller, S. J., Stone, D., Whalley, L. K., and Heard, D. E.: OH reactivity in a South East Asian tropical rainforest during the Oxidant and Particle Photochemical Processes (OP3) project, Atmos. Chem. Phys., 13, 9497–9514, doi:10.5194/acp-13-9497-2013, 2013.
Faloona, I., Tan, D., Brune, W., Hurst, J., Barket, D., Couch, T. L., Shepson, P., Apel, E., Riemer, D., Thornberry, T., Carroll, M. A., Sillman, S., Keeler, G. J., Sagady, J., Hooper, D., and Paterson, K.: Nighttime observations of anomalously high levels of hydroxyl radicals above a deciduous forest canopy, J. Geophys. Res.-Atmos., 106, 24315–24333, 2001.
Farmer, D. K., Perring, A. E., Wooldridge, P. J., Blake, D. R., Baker, A., Meinardi, S., Huey, L. G., Tanner, D., Vargas, O., and Cohen, R. C.: Impact of organic nitrates on urban ozone production, Atmos. Chem. Phys., 11, 4085–4094, doi:10.5194/acp-11-4085-2011, 2011.
Fry, J. L., Draper, D. C., Zarzana, K. J., Campuzano-Jost, P., Day, D. A., Jimenez, J. L., Brown, S. S., Cohen, R. C., Kaser, L., Hansel, A., Cappellin, L., Karl, T., Hodzic Roux, A., Turnipseed, A., Cantrell, C., Lefer, B. L., and Grossberg, N.: Observations of gas- and aerosol-phase organic nitrates at BEACHON-RoMBAS 2011, Atmos. Chem. Phys., 13, 8585–8605, doi:10.5194/acp-13-8585-2013, 2013.
Fuchs, H., Bohn, B., Hofzumahaus, A., Holland, F., Lu, K. D., Nehr, S., Rohrer, F., and Wahner, A.: Detection of HO_2 by laser-induced fluorescence: calibration and interferences from RO_2 radicals, Atmos. Meas. Tech., 4, 1209–1225, doi:10.5194/amt-4-1209-2011, 2011.
Goldstein, A. H., McKay, M., Kurpius, M. R., Schade, G. W., Lee, A., Holzinger, R., and Rasmussen, R. A.: Forest thinning experiment confirms ozone deposition to forest canopy is dominated by reaction with biogenic VOCs, Geophys. Res. Lett., 31, L22106, doi:10.1029/2004GL021259, 2004.

Griffith, S. M., Hansen, R. F., Dusanter, S., Stevens, P. S., Alaghmand, M., Bertman, S. B., Carroll, M. A., Erickson, M., Galloway, M., Grossberg, N., Hottle, J., Hou, J., Jobson, B. T., Kammrath, A., Keutsch, F. N., Lefer, B. L., Mielke, L. H., O'Brien, A., Shepson, P. B., Thurlow, M., Wallace, W., Zhang, N., and Zhou, X. L.: OH and HO_2 radical chemistry during PROPHET 2008 and CABINEX 2009 – Part 1: Measurements and model comparison, Atmos. Chem. Phys., 13, 5403–5423, doi:10.5194/acp-13-5403-2013, 2013.

Guenther, A. B., Jiang, X., Heald, C. L., Sakulyanontvittaya, T., Duhl, T., Emmons, L. K., and Wang, X.: The Model of Emissions of Gases and Aerosols from Nature version 2.1 (MEGAN2.1): an extended and updated framework for modeling biogenic emissions, Geosci. Model Dev., 5, 1471–1492, doi:10.5194/gmd-5-1471-2012, 2012.

Hallquist, M., Wenger, J. C., Baltensperger, U., Rudich, Y., Simpson, D., Claeys, M., Dommen, J., Donahue, N. M., George, C., Goldstein, A. H., Hamilton, J. F., Herrmann, H., Hoffmann, T., Iinuma, Y., Jang, M., Jenkin, M. E., Jimenez, J. L., Kiendler-Scharr, A., Maenhaut, W., McFiggans, G., Mentel, Th. F., Monod, A., Prévôt, A. S. H., Seinfeld, J. H., Surratt, J. D., Szmigielski, R., and Wildt, J.: The formation, properties and impact of secondary organic aerosol: current and emerging issues, Atmos. Chem. Phys., 9, 5155–5236, doi:10.5194/acp-9-5155-2009, 2009.

Harley, P., Fridd-Stroud, V., Greenberg, J., Guenther, A., and Vasconcellos, P.: Emission of 2-methyl-3-buten-2-ol by pines: a potentially large natural source of reactive carbon to the atmosphere, J. Geophys. Res., 103, 25479–25486, 1998.

Hewitt, C. N., Kok, G. L., and Fall, R.: Hydroperoxides in plants exposed to ozone mediate air pollution damage to alkene emitters, Nature, 344, 56–57, 1990.

Hofzumahaus, A., Rohrer, F., Lu, K., Bohn, B., Brauers, T., Chang, C.-C., Fuchs, H., Holland, F., Kita, K., Kondo, Y., Li, X., Lou, S., Shao, M., Zeng, L., Wahner, A., and Zhang, Y.: Amplified trace gas removal in the troposphere, Science, 324, 1702–1704, doi:10.1126/science.1164566, 2009.

Hogg, A., Uddling, J., Ellsworth, D., Carroll, M. A., Pressley, S., Lamb, B., and Vogel, C.: Stomatal and non-stomatal fluxes of ozone to a northern mixed hardwood forest, Tellus B, 59, 514–525, 2007.

Holzinger, R., Lee, A., Paw, K. T., and Goldstein, U. A. H.: Observations of oxidation products above a forest imply biogenic emissions of very reactive compounds, Atmos. Chem. Phys., 5, 67–75, doi:10.5194/acp-5-67-2005, 2005.

Hornbrook, R. S., Crawford, J. H., Edwards, G. D., Goyea, O., Mauldin III, R. L., Olson, J. S., and Cantrell, C. A.: Measurements of tropospheric HO_2 and RO_2 by oxygen dilution modulation and chemical ionization mass spectrometry, Atmos. Meas. Tech., 4, 735–756, doi:10.5194/amt-4-735-2011, 2011.

Jenkin, M. E., Saunders, S. M., and Pilling, M. J.: The tropospheric degradation of volatile organic compounds: a protocol for mechanism development, Atmos. Environ., 31, 81–104, 1997.

Karl, T., Hansel, A., Cappellin, L., Kaser, L., Herdlinger-Blatt, I., and Jud, W.: Selective measurements of isoprene and 2-methyl-3-buten-2-ol based on NO^+ ionization mass spectrometry, Atmos. Chem. Phys., 12, 11877–11884, doi:10.5194/acp-12-11877-2012, 2012.

Kaser, L., Karl, T., Guenther, A., Graus, M., Schnitzhofer, R., Turnipseed, A., Fischer, L., Harley, P., Madronich, M., Gochis, D., Keutsch, F. N., and Hansel, A.: Undisturbed and disturbed above canopy ponderosa pine emissions: PTR-TOF-MS measurements and MEGAN 2.1 model results, Atmos. Chem. Phys. Discuss., 13, 15333–15375, doi:10.5194/acpd-13-15333-2013, 2013a.

Kaser, L., Karl, T., Schnitzhofer, R., Graus, M., Herdlinger-Blatt, I. S., DiGangi, J. P., Sive, B., Turnipseed, A., Hornbrook, R. S., Zheng, W., Flocke, F. M., Guenther, A., Keutsch, F. N., Apel, E., and Hansel, A.: Comparison of different real time VOC measurement techniques in a ponderosa pine forest, Atmos. Chem. Phys., 13, 2893–2906, doi:10.5194/acp-13-2893-2013, 2013b.

Kim, S., Wolfe, G. M., Mauldin, L., Cantrell, C., Guenther, A., Karl, T., Turnipseed, A., Greenberg, J., Hall, S. R., Ullmann, K., Apel, E., Hornbrook, R., Kajii, Y., Nakashima, Y., Keutsch, F. N., DiGangi, J. P., Henry, S. B., Kaser, L., Schnitzhofer, R., Graus, M., Hansel, A., Zheng, W., and Flocke, F. F.: Evaluation of HO_x sources and cycling using measurement-constrained model calculations in a 2-methyl-3-butene-2-ol (MBO) and monoterpene (MT) dominated ecosystem, Atmos. Chem. Phys., 13, 2031–2044, doi:10.5194/acp-13-2031-2013, 2013.

Kirchner, F., Mayer-Figge, A., Zabel, F., and Becker, K. H.: Thermal stability of peroxynitrates, Int. J. Chem. Kinet., 31, 127–144, 1999.

Kurpius, M. R. and Goldstein, A. H.: Gas-phase chemistry dominates O_3 loss to a forest, implying a source of aerosols and hydroxyl radicals to the atmosphere, Geophys. Res. Lett., 30, 1371–1374, doi:10.1029/2002GL016785, 2003.

LaFranchi, B. W., Wolfe, G. M., Thornton, J. A., Harrold, S. A., Browne, E. C., Min, K. E., Wooldridge, P. J., Gilman, J. B., Kuster, W. C., Goldan, P. D., de Gouw, J. A., McKay, M., Goldstein, A. H., Ren, X., Mao, J., and Cohen, R. C.: Closing the peroxy acetyl nitrate budget: observations of acyl peroxy nitrates (PAN, PPN, and MPAN) during BEARPEX 2007, Atmos. Chem. Phys., 9, 7623–7641, doi:10.5194/acp-9-7623-2009, 2009.

Lelieveld, J., Butler, T. M., Crowley, J. N., Dillon, T. J., Fischer, H., Ganzeveld, L., Harder, H., Lawrence, M. G., Martinez, M., Taraborrelli, D., and Williams, J.: Atmospheric oxidation capacity sustained by a tropical forest, Nature, 452, 737–740, doi:10.1038/nature06870, 2008.

Liu, Y. J., Herdlinger-Blatt, I., McKinney, K. A., and Martin, S. T.: Production of methyl vinyl ketone and methacrolein via the hydroperoxyl pathway of isoprene oxidation, Atmos. Chem. Phys., 13, 5715–5730, doi:10.5194/acp-13-5715-2013, 2013.

Lou, S., Holland, F., Rohrer, F., Lu, K., Bohn, B., Brauers, T., Chang, C.C., Fuchs, H., Häseler, R., Kita, K., Kondo, Y., Li, X., Shao, M., Zeng, L., Wahner, A., Zhang, Y., Wang, W., and Hofzumahaus, A.: Atmospheric OH reactivities in the Pearl River Delta – China in summer 2006: measurement and model results, Atmos. Chem. Phys., 10, 11243–11260, doi:10.5194/acp-10-11243-2010, 2010.

Makar, P. A., Fuentes, J. D., Wang, D., Staebler, R. M., and Wiebe, H. A.: Chemical processing of biogenic hydrocarbons within and above a temperate deciduous forest, J. Geophys. Res., 104, 3581–3603, 1999.

Mauldin, R., Berndt, T., Sipila, M., Paasonen, P., Petaja, T., Kim, S., Kurten, T., Stratmann, F., Kerminen, V., and Kulmala, M.: A new atmospherically relevant oxidant of sulphur dioxide, Nature, 488, 193–197, doi:10.1038/nature11278, 2012.

Mihele, C. M. and Hastie, D. R.: Radical chemistry at a forested continental site: Results from the PROPHET 1997 campaign, J. Geophys. Res., 108, 4450–4460, doi:10.1029/2002JD002888, 2003.

Moxim, W. J., Levy II, H., and Kasibhatla, P. S.: Simulated global tropospheric PAN: Its transport and impact on NO_x, J. Geophys. Res., 101, 12621–12638, 1996.

Nakashima, Y., Ida, A., Yoshino, A., Suthawaree, J., Kato, S., Greenberg, J., Kim, S., Karl, T., Turnipseed, A., Guenther, A., DiGangi, J. P., Henry, S., Keutsch, F. N., Schnitzhofer, R., Kaser, L., Graus, M., Hansel, A., and Kajii, Y.: Total OH reactivity measurements at the Manitou Experimental Forest in summer season during BEACHON-ROCS campaign, in preparation, 2013.

Nölscher, A. C., Williams, J., Sinha, V., Custer, T., Song, W., Johnson, A. M., Axinte, R., Bozem, H., Fischer, H., Pouvesle, N., Phillips, G., Crowley, J. N., Rantala, P., Rinne, J., Kulmala, M., Gonzales, D., Valverde-Canossa, J., Vogel, A., Hoffmann, T., Ouwersloot, H. G., Vilà-Guerau de Arellano, J., and Lelieveld, J.: Summertime total OH reactivity measurements from boreal forest during HUMPPA-COPEC 2010, Atmos. Chem. Phys., 12, 8257–8270, doi:10.5194/acp-12-8257-2012, 2012.

Paulot, F., Henze, D. K., and Wennberg, P. O.: Impact of the isoprene photochemical cascade on tropical ozone, Atmos. Chem. Phys., 12, 1307–1325, doi:10.5194/acp-12-1307-2012, 2012.

Peeters, J. and Müller, J. F.: HO_x radical regeneration in isoprene oxidation via peroxy radical isomerisations, II: experimental evidence and global impact, Phys. Chem. Chem. Phys., 12, 14227–14235, 2010.

Peeters, J., Nguyen, T. L., and Vereecken, L.: HO_x radical regeneration in the oxidation of isoprene, Phys. Chem. Chem. Phys., 11, 5935–5939, 2009.

Qi, B., Takami, A., and Hatakeyama, S.: Peroxy radical concentrations measured at a forest canopy in Nikko, Japan, in summer 2002, J. Atmos. Chem., 52, 63–79, 2005.

Ren, X. R., Olson, J. R., Crawford, J. H., Brune, W. H., Mao, J. Q., Long, R. B., Chen, Z., Chen, G., Avery, M. A., Sachse, G. W., Barrick, J. D., Diskin, G. S., Huey, L. G., Fried, A., Cohen, R. C., Heikes, B., Wennberg, P. O., Singh, H. B., Blake, D. R., and Shetter, R. E.: HO_x chemistry during INTEX-A 2004: Observation, model calculation, and comparison with previous studies, J. Geophys. Res.-Atmos., 113, D05310, doi:10.1029/2003JD003551, 2008.

Saunders, S. M., Jenkin, M. E., Derwent, R. G., and Pilling, M. J.: Protocol for the development of the Master Chemical Mechanism, MCM v3 (Part A): tropospheric degradation of non-aromatic volatile organic compounds, Atmos. Chem. Phys., 3, 161–180, doi:10.5194/acp-3-161-2003, 2003.

Seok, B., Helmig, D., Ganzeveld, L., Williams, M. W., and Vogel, C. S.: Dynamics of nitrogen oxides and ozone above and within a mixed hardwood forest in northern Michigan, Atmos. Chem. Phys., 13, 7301–7320, doi:10.5194/acp-13-7301-2013, 2013.

Shu, Y. and Atkinson, R.: Rate constants for the gas-phase reactions of O_3 with a series of terpenes and OH radical formation from the O_3 reactions with sesquiterpenes at 296 ± 2 K, Int. J. Chem. Kinet., 26, 1193–1205, 1994.

Sinha, V., Williams, J., Lelieveld, J., Ruuskanen, T. M., Kajos, M. K., Patokoski, J., Hellen, H., Hakola, H., Mogensen, D., Boy, M., Rinne, J., and Kulmala, M.: OH reactivity measurements

within a boreal forest: evidence for unknown reactive emissions, Environ. Sci. Technol., 44, 6614–6620, 2010.

Sommariva, R., Bates, T. S., Bon, D., Brookes, D. M., de Gouw, J. A., Gilman, J. B., Herndon, S. C., Kuster, W. C., Lerner, B. M., Monks, P. S., Osthoff, H. D., Parker, A. E., Roberts, J. M., Tucker, S. C., Warneke, C., Williams, E. J., Zahniser, M. S., and Brown, S. S.: Modelled and measured concentrations of peroxy radicals and nitrate radical in the US Gulf Coast region during TexAQS 2006, J. Atmos. Chem., 68, 331–362, doi:10.1007/s10874-012-9224-7, 2011.

Sparks, J. P., Walker, J., Turnipseed, A., and Guenther, A.: Dry nitrogen deposition estimates over a forest experiencing free air CO_2 enrichment, Glob. Change Biol., 14, 768–781, 2008.

Stavrakou, T., Peeters, J., and Müller, J.-F.: Improved global modelling of HO_x recycling in isoprene oxidation: evaluation against the GABRIEL and INTEX-A aircraft campaign measurements, Atmos. Chem. Phys., 10, 9863–9878, doi:10.5194/acp-10-9863-2010, 2010.

Stone, D., Whalley, L. K., and Heard, D. E.: Tropospheric OH and HO_2 radicals: field measurements and model comparisons, Chem. Soc. Rev., 41, 6348–6404, doi:10.1039/C2CS35140D, 2012.

Tan, D., Faloona, I., Simpas, J. B., Brune, W., Shepson, P. B., Couch, T. L., Sumner, A. L., Carroll, M. A., Thornberry, T., Apel, E., Riemer, D., and Stockwell, W.: HO_x budgets in a deciduous forest: results from the PROPHET summer 1998 campaign, J. Geophys. Res. Atmos., 106, 24407–24427, 2001.

Thornton, J. A., Wooldridge, P. J., Cohen, R. C., Martinez, M., Harder, H., Brune, W. H., Williams, E. J., Roberts, J. M., Fehsenfeld, F. C., Hall, S. R., Shetter, R. E., Wert, B. P., and Fried, A.: Ozone production rates as a function of NO_x abundances and HO_x production rates in the Nashville urban plume, J. Geophys. Res., 107, 4146–4163, doi:10.1029/2001JD000932, 2002.

Whalley, L. K., Edwards, P. M., Furneaux, K. L., Goddard, A., Ingham, T., Evans, M. J., Stone, D., Hopkins, J. R., Jones, C. E., Karunaharan, A., Lee, J. D., Lewis, A. C., Monks, P. S., Moller, S. J., and Heard, D. E.: Quantifying the magnitude of a missing hydroxyl radical source in a tropical rainforest, Atmos. Chem. Phys., 11, 7223–7233, doi:10.5194/acp-11-7223-2011, 2011.

Whalley, L. K., Blitz, M. A., Desservettaz, M., Seakins, P. W., and Heard, D. E.: Reporting the sensitivity of Laser Induced Fluorescence instruments used for HO_2 detection to an interference from RO_2 radicals and introducing a novel approach that enables HO_2 and certain RO_2 types to be selectively measured, Atmos. Meas. Tech. Discuss., 6, 6249–6292, doi:10.5194/amtd-6-6249-2013, 2013.

Wolfe, G. M. and Thornton, J. A.: The Chemistry of Atmosphere-Forest Exchange (CAFE) Model – Part 1: Model description and characterization, Atmos. Chem. Phys., 11, 77–101, doi:10.5194/acp-11-77-2011, 2011.

Wolfe, G. M., Thornton, J. A., Bouvier-Brown, N. C., Goldstein, A. H., Park, J.-H., McKay, M., Matross, D. M., Mao, J., Brune, W. H., LaFranchi, B. W., Browne, E. C., Min, K.-E., Wooldridge, P. J., Cohen, R. C., Crounse, J. D., Faloona, I. C., Gilman, J. B., Kuster, W. C., de Gouw, J. A., Huisman, A., and Keutsch, F. N.: The Chemistry of Atmosphere-Forest Exchange (CAFE) Model – Part 2: Application to BEARPEX-2007 observations, Atmos. Chem. Phys., 11, 1269–1294, doi:10.5194/acp-11-1269-2011, 2011a.

Wolfe, G. M., Thornton, J. A., McKay, M., and Goldstein, A. H.: Forest-atmosphere exchange of ozone: sensitivity to very reactive biogenic VOC emissions and implications for in-canopy photochemistry, Atmos. Chem. Phys., 11, 7875–7891, doi:10.5194/acp-11-7875-2011, 2011b.

Wolfe, G. M., Crounse, J. D., Parrish, J. D., St. Clair, J. M., Beaver, M. R., Paulot, F., Yoon, T. P., Wennberg, P. O., and Keutsch, F. N.: Photolysis, OH reactivity and ozone reactivity of a proxy for isoprene-derived hydroperoxyenals (HPALDs), Phys. Chem. Chem. Phys., 14, 7276–7286, doi:10.1039/C2CP40388A, 2012.

Wooldridge, P. J., Perring, A. E., Bertram, T. H., Flocke, F. M., Roberts, J. M., Singh, H. B., Huey, L. G., Thornton, J. A., Wolfe, G. M., Murphy, J. G., Fry, J. L., Rollins, A. W., LaFranchi, B. W., and Cohen, R. C.: Total Peroxy Nitrates (ΣPNs) in the atmosphere: the Thermal Dissociation-Laser Induced Fluorescence (TD-LIF) technique and comparisons to speciated PAN measurements, Atmos. Meas. Tech., 3, 593–607, doi:10.5194/amt-3-593-2010, 2010.

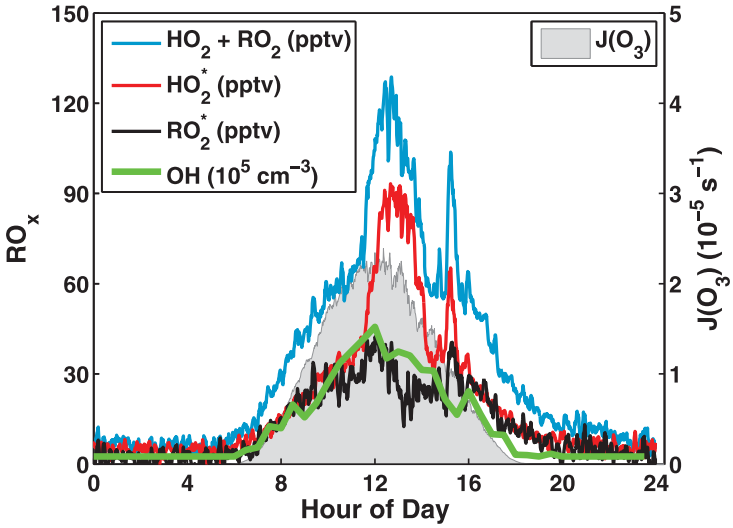

Fig. 1. Average diel cycles of total peroxy radicals (blue), HO_2^* (red), RO_2^* (black), OH (green) and ozone photolysis frequency (filled gray area). Peroxy radicals and $J(O_3)$ are shown as 1 min means, while OH is displayed as a 30 min mean. $J(O_3)$ is calculated by scaling measured $J(NO_2)$ with the ratio of $J(O_3)/J(NO_2)$ calculated from the MCM parameterization for clear-sky conditions. Nighttime OH values were typically below the instrument detection limit ($5 \times 10^5 cm^{-3}$) and are thus set to half of this value.

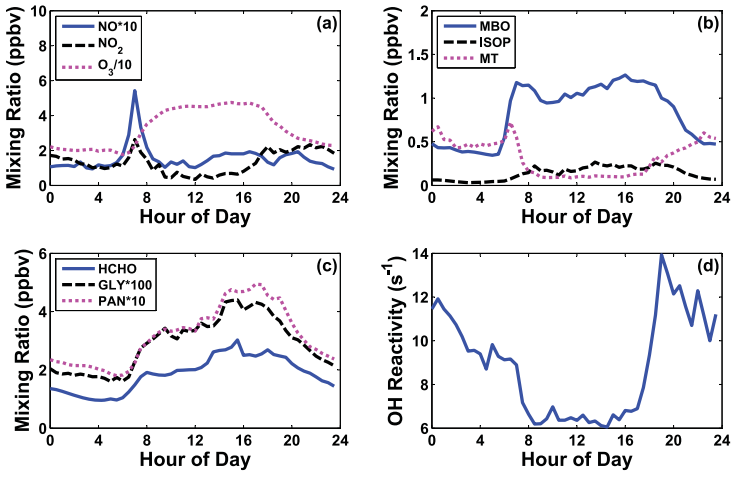

Fig. 2. Average diel observations of **(a)** NO, NO_2 and ozone, **(b)** MBO, isoprene and total monoterpenes, **(c)** formaldehyde, glyoxal and PAN, and **(d)** OH reactivity. All data are 30 min means. Note that some species have been scaled to fit on a single axis, as denoted in the plot legends.

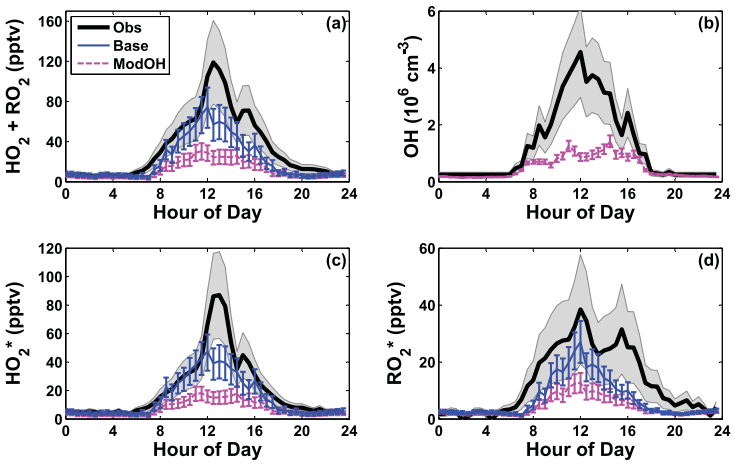

Fig. 3. Comparison of RO_x observations with 0-D model results. Solid black lines with shaded gray areas represent observations and their associated uncertainties. Model scenarios include the base (solid blue line) and ModOH (dashed magenta line) simulations; in the latter case, OH concentrations are not constrained to observations. For comparison with HO_2^* and RO_2^* in **(c)** and **(d)**, the total modeled RO_2 is sub-divided into two groups as described in the text. Calculation of model uncertainties is described in the SI.

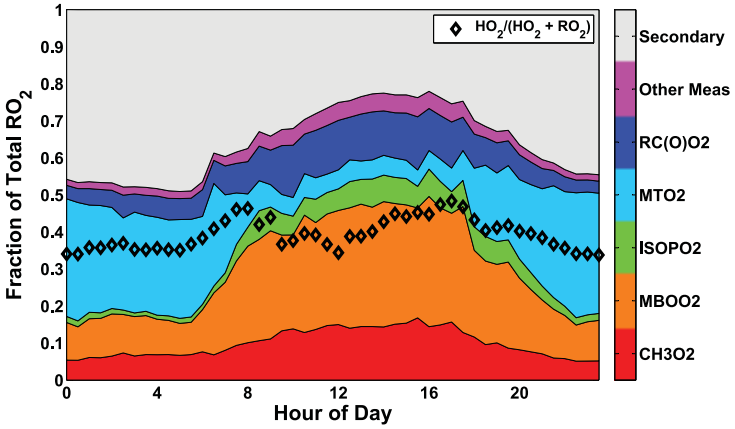

Fig. 4. Modeled distribution of organic peroxy radicals from the base simulation. Groups include methyl peroxy radical (red), first-generation peroxy radicals of MBO (yellow), isoprene (green) and monoterpenes (cyan), total acyl peroxy radicals (blue), first-generation radicals from oxidation of other measured VOC (magenta), and "secondary" radicals resulting from oxidation of model-predicted, unmeasured VOC (gray). The ratio of HO_2 to total peroxy radicals is also shown (black diamonds).

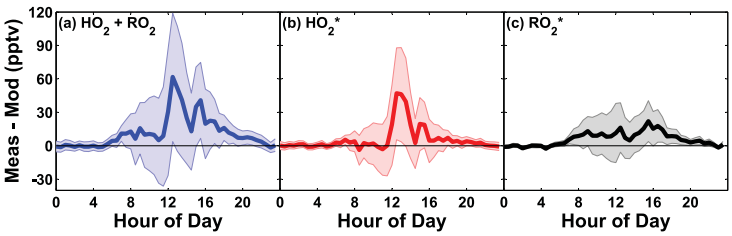

Fig. 5. Difference between observed and modeled peroxy radical mixing ratios: **(a)** total peroxy radicals, **(b)** HO_2^* and **(c)** RO_2^*. Model values are taken from the base simulation. Shaded areas represent the combined uncertainty from observed and modeled mixing ratios.

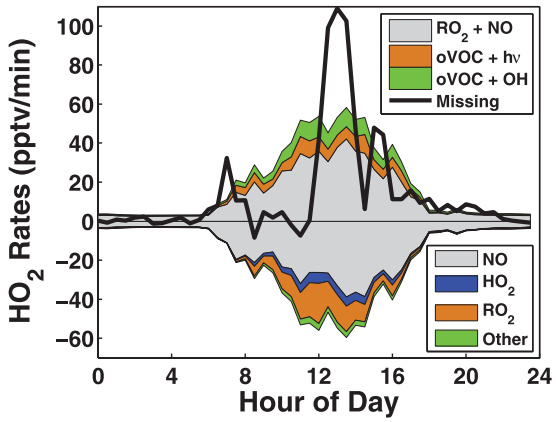

Fig. 6. Rates of HO_2 production and loss calculated from the base model scenario. Rates are grouped according to the type of reaction. Production includes reaction of RO_2 with NO (gray), VOC photolysis (orange) and OH oxidation of VOC (green). Losses include reactions with NO (gray), HO_2 (blue), RO_2 (orange) and OH and ozone (green). The thick black line denotes the proposed missing HO_2 source, calculated as described in the text.

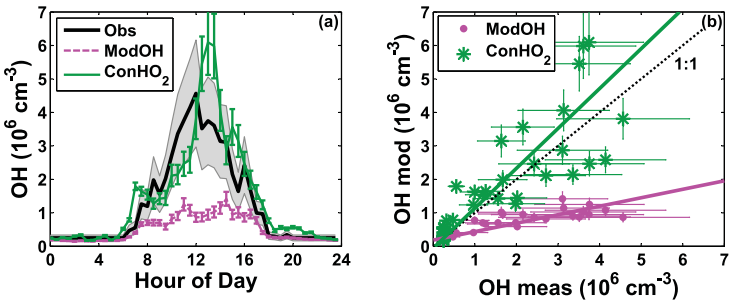

Fig. 7. Comparison of measured and modeled OH concentrations. **(a)** Diurnal profiles. Observations and their uncertainties are shown as a black line with grey shading. The ModOH results (magenta) are the same as those shown in Fig. 3. In the HO_2-constrained case (green), HO_2 is constrained to "missing" HO_2^* as described in Sect. 5.1. The same uncertainties are assumed for both model scenarios. **(b)** Scatter plot of the same results for ModOH (magenta dots) and HO_2-constrained (green asterisks) scenarios. Thins lines define uncertainties in modeled and measured values. Thick lines represent uncertainty-weighted major axis regression fits (ModOH: $y = 0.24x + 0.18$, $r^2 = 0.81$; ConHO$_2$: $y = 1.19x - 0.05$, $r^2 = 0.75$).

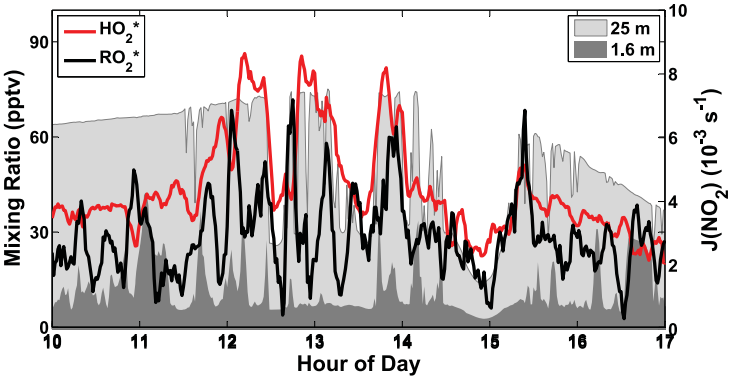

Fig. 8. Example of fast mid-day variations of solar radiation and peroxy radicals for day 234 (22 August). HO_2^* (red) and RO_2^* (black) are plotted on the left axis, while NO_2 photolysis frequencies are plotted on the right axis for both above-canopy (light gray) and below-canopy (dark gray) measurements. All data are 1 min averages.

Discussion Paper | Discussion Paper | Discussion Paper | Discussion Paper |

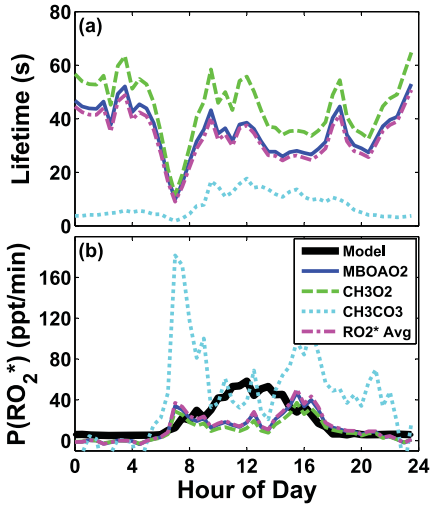

Fig. 9. (a) Modeled chemical lifetimes for several representative species: MBOAO2 (solid blue line), methyl peroxy radical (dashed green line) and acetyl peroxy radical (dashed cyan line). The concentration-weighted average RO_2^* lifetime is also shown (dash-dotted magenta line). **(b)** Missing RO_2^* production rates calculated as described in the text. Also shown is the total production rate for all modeled RO_2^*(thick black line). Model results are taken from the base simulation.

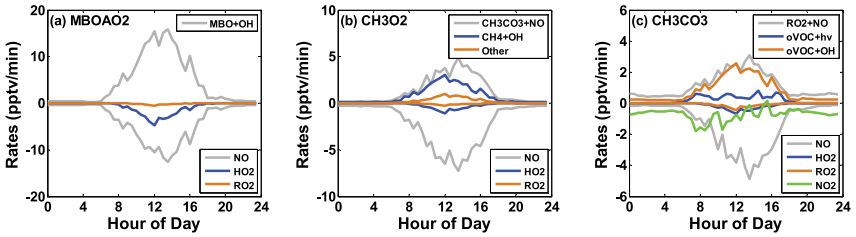

Fig. 10. Modeled chemical tendencies for three representative organic peroxy radicals: **(a)** MBOAO2, **(b)** methyl peroxy radical and **(c)** acetyl peroxy radical. In **(c)**, the loss rate attributed to NO_2 (green line) represents the net effect of PAN production and decomposition. Model results are taken from the base simulation.

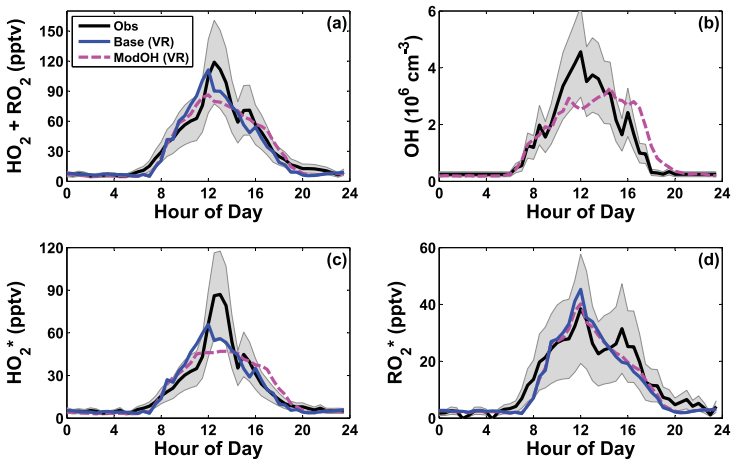

Fig. 11. Comparison of RO_x observations with 0-D model results using the very reactive VOC mechanism. Solid black lines with shaded gray areas represent observations and their associated uncertainties. Model simulations include the base (solid blue line) and ModOH (dashed magenta line) scenarios augmented with very reactive VOC chemistry; in the latter case, OH concentrations are not constrained to observations. For comparison with HO_2^* and RO_2^* in **(c)** and **(d)**, the total modeled RO_2 is sub-divided into two groups as described in the text. Model uncertainties are excluded for clarity.